Supplementary file

Fluid-pore relationships in tight oil shales: Insights from sequential solvent extraction and advanced rock analysis

Aliya Mukhametdinova[1]*, Bogdan Andreyev[1], Daria Sergeeva[1], Alexander Burukhin[1], Georgy Kalmykov[2], Anton Kalmykov[2], and Alexey Cheremisin[1]

[1]*Center for Petroleum Science and Engineering, Skolkovo Institute of Science and Technology, Moscow 121205, Russia*

[2]*Faculty of Geology, Lomonosov Moscow State University, University, Moscow 119991, Russia*

E-mail address: a.mukhametdinova@skoltech.ru (A. Mukhametdinova); bogdan.andreyev@skoltech.ru (B. Andreyev); d.sergeeva@skoltech.ru (D. Sergeeva); a.burukhin@skoltech.ru (A. Burukhin); gera64@mail.ru (G. Kalmykov); a.kalmykov@oilmsu.ru (A. Kalmykov); a.cheremisin@skoltech.ru (A. Cheremisin).

*Corresponding author (ORCID: 0000-0001-7270-4806 (A. Mukhametdinova))

Mukhametdinova, A., Andreyev, B., Sergeeva, D., Burukhin, A., Kalmykov G., Kalmykov A., Cheremisin, A. Fluid-pore relationships in tight oil shales: Insights from sequential solvent extraction and advanced rock analysis. Advances in Geo-Energy Research, 2026, 20(3): 243-258.

The link to this file is: https://doi.org/10.46690/ager.2026.06.06

Appendix A: Figures

Four distinct lithotypes were identified in the investigated collection of Bazhenov Formation samples through an integrated analysis of thin sections as shown in Fig. S1.

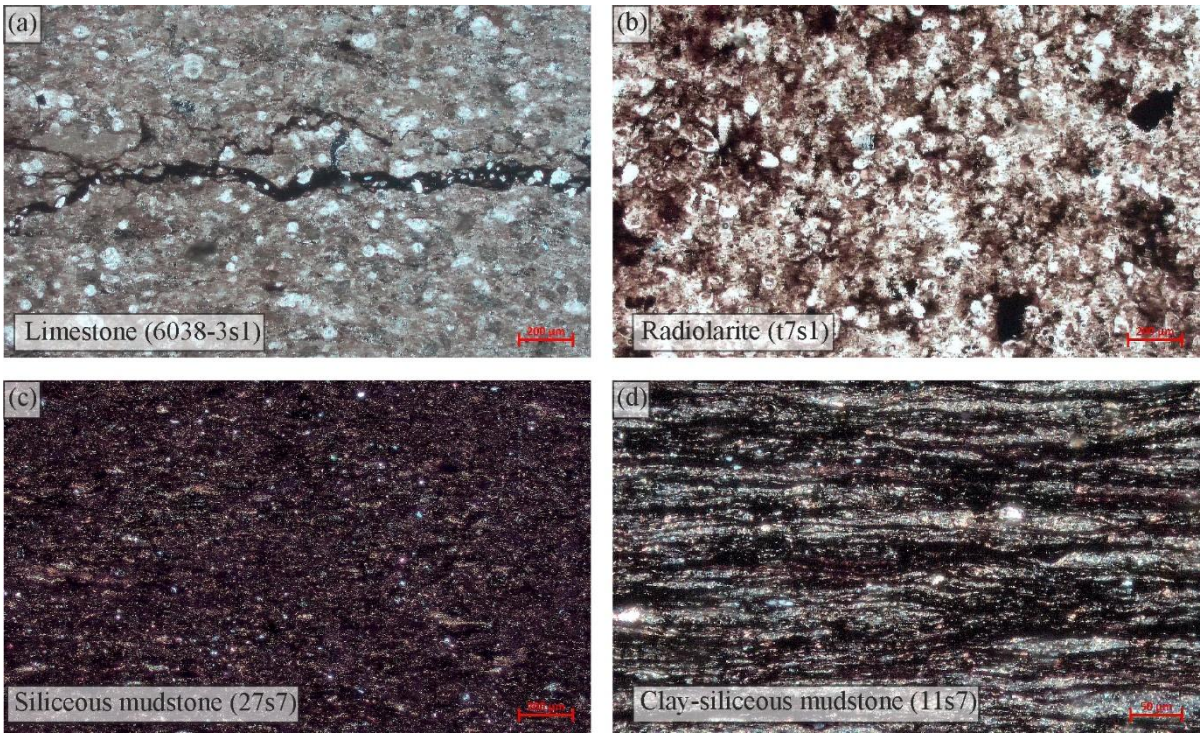

Fig. S1. Thin-section images of the main lithotypes: (a) limestone, (b) radiolarite, (c) siliceous mudstone, (d) clay-siliceous mudstone.

Processing the results of the standard and Xe-saturated μCT images by subtracting the original image from the Xe-saturated one provided a map of contrast agent propagation, which could be used as equivalent to an open porosity map as shown in Fig. S2. Concentration of Xe penetrated the sample is highlighted in color.

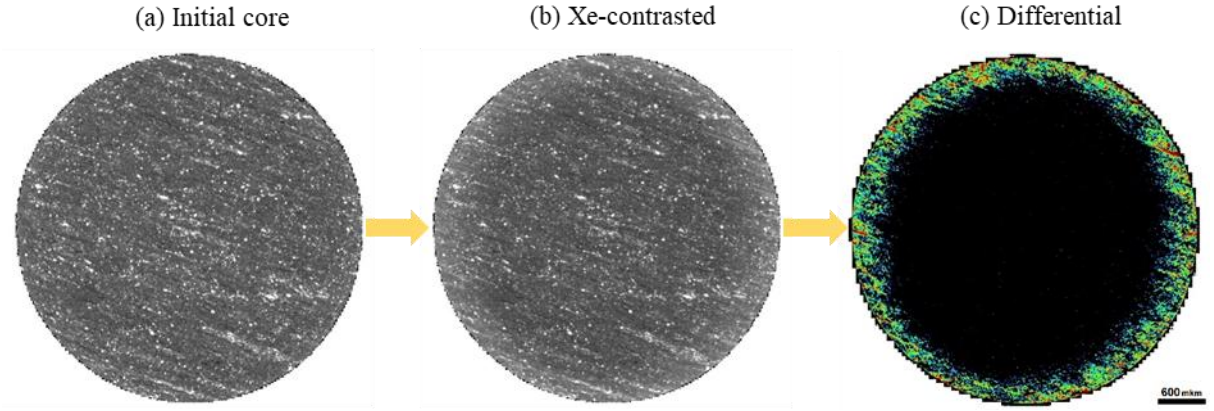

Fig. S2. Images of t2s1 sample (Ø4 mm): (a) Initial (as-received), (b) Xe-saturated after 1st step of extraction and (c) differential.

Differential images for rock samples in Fig. S3 showed that the initial open porosity can be very limited (e.g., samples 11s3, t2s1) or fragmented and localized (e.g., samples 11s7, 25s5, 25s6)

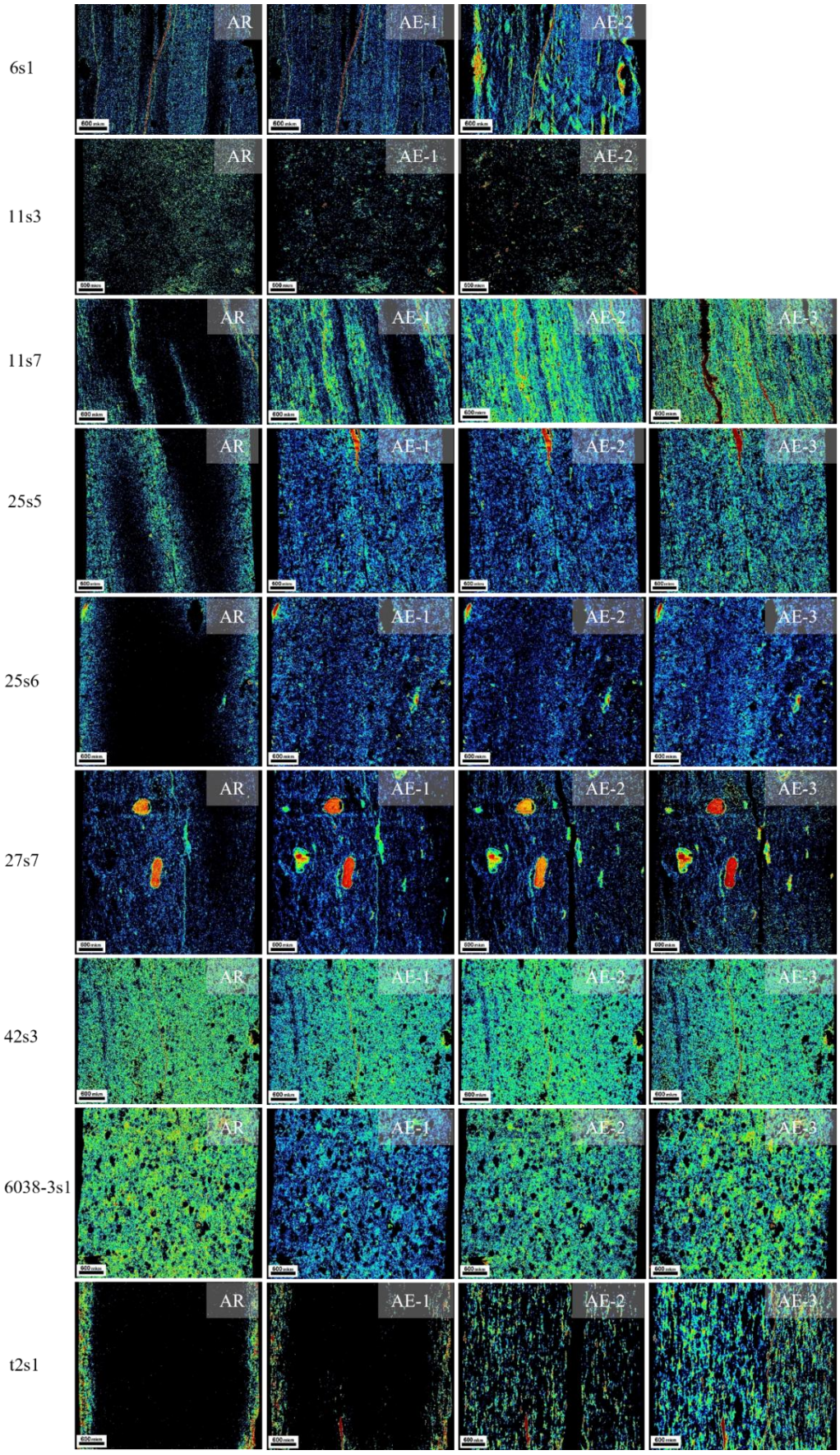

Fig. S3. Microtomography differential images for entire collection in different states.

Fig. S4 demonstrates the change of mini core porosity by µCT at each stage of the workflow. The µCT analysis confirms that chloroform extraction (AE-2) is necessary to approach true open porosity values.

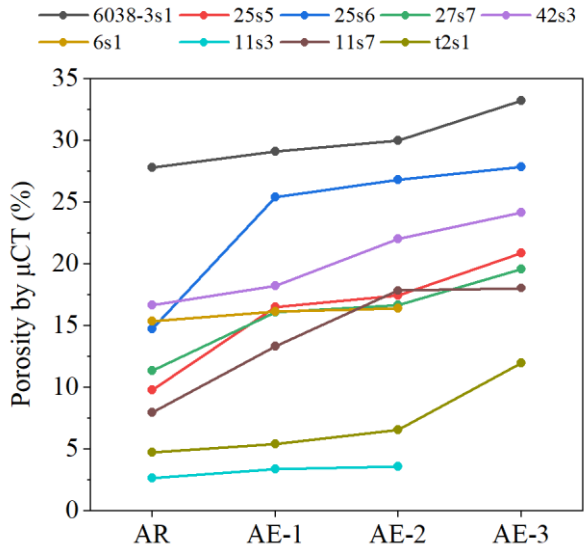

Fig. S4. Segmented porosity of samples by µCT for Xe-saturated samples (Ø4 mm) in as-received state (AR), after the consequent extraction with hexane (AE-1), chloroform (AE-2), and alcohol-benzene mixture (AE-3).

The PSD registered by µCT at the given resolution can provide insights into pore space evolution in macroscale porosity range within the multistage solvent extraction, as illustrated for the samples t2s1, 11s7, and 27s7 in Fig. S5.

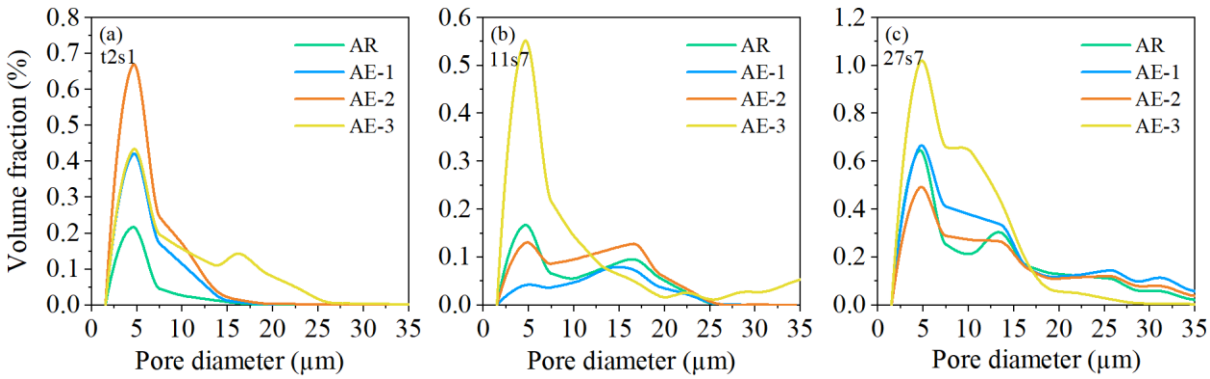

Fig. S5. Pore size distribution for selected samples in different states of solvent extraction as well as initial state: (a) Sample t2s1, (b) sample 11s7, (c) sample 27s7.

For detailed analysis of the fluid removal and its redistribution in the pore structure, the T2-based PSD for selected samples was generated based on the T_2 relaxation curves as shown in Fig. S6.

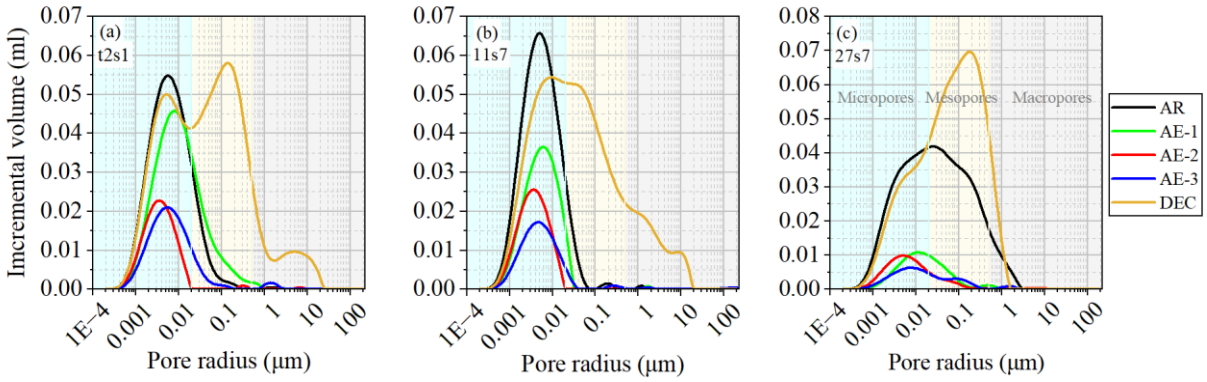

Fig. S6. Pore size distribution by T_2 analysis: (a) sample t2s1, (b) sample 11s7, (c) sample 27s7.

The comparison of AR and DEC maps in Fig. S7 suggests the development of pore network not only by means of HCs cleaning but also by expansion of porosity caused by the technogenic reasons.

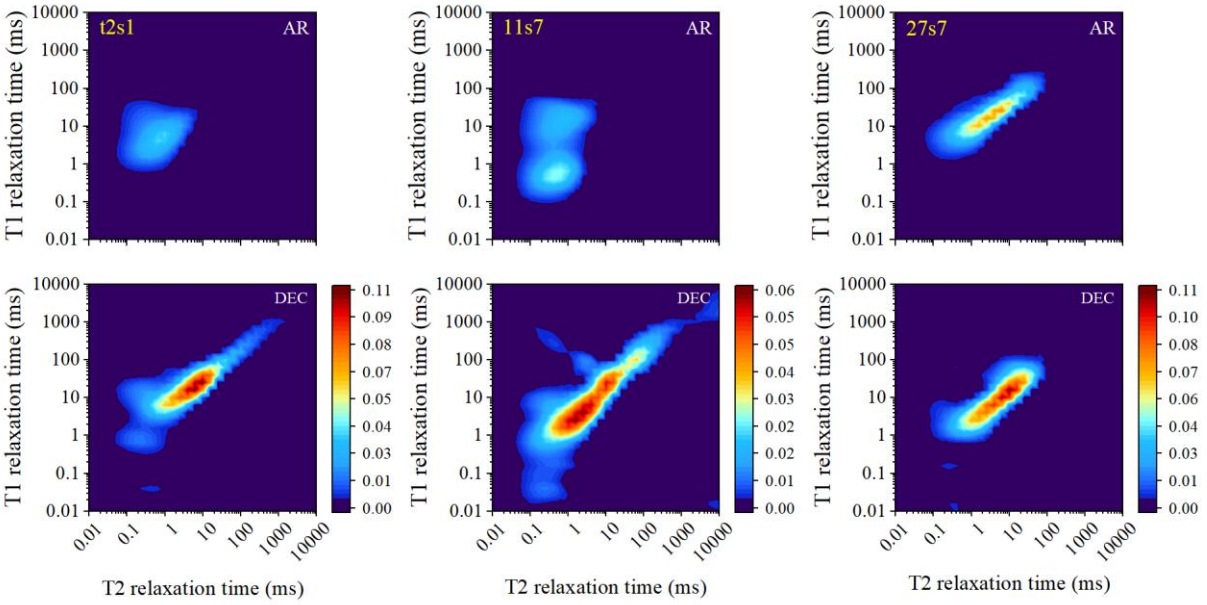

Fig. S7. T_1-T_2 maps for selected samples in AR and DEC stages.

Fig. S8 illustrates that most hydrocarbons in the rock were removed during AE-1 step using

hexane for mature samples. The chloroform proved its efficiency in subsequent core cleaning, especially for low mature clay-siliceous and siliceous mudstone samples with high TOC and clay content.

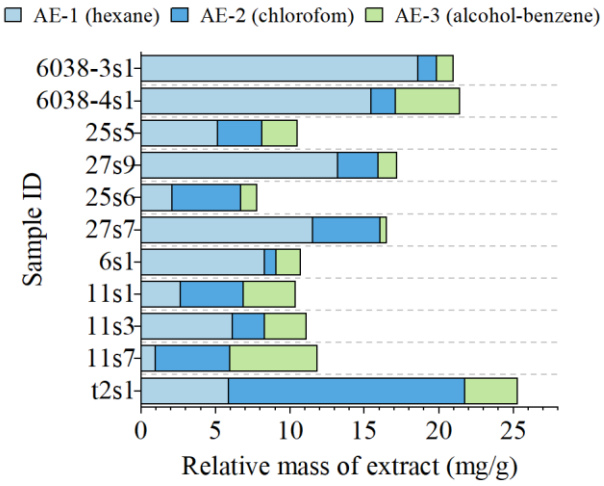

Fig. S8. Change of extract mass during the multistep core extraction.

Importantly, effective porosity does not correlate with quartz abundance (as shown in Fig. S9), suggesting that soft components (swelling clays, OM) govern porosity more than rigid mineral frameworks.

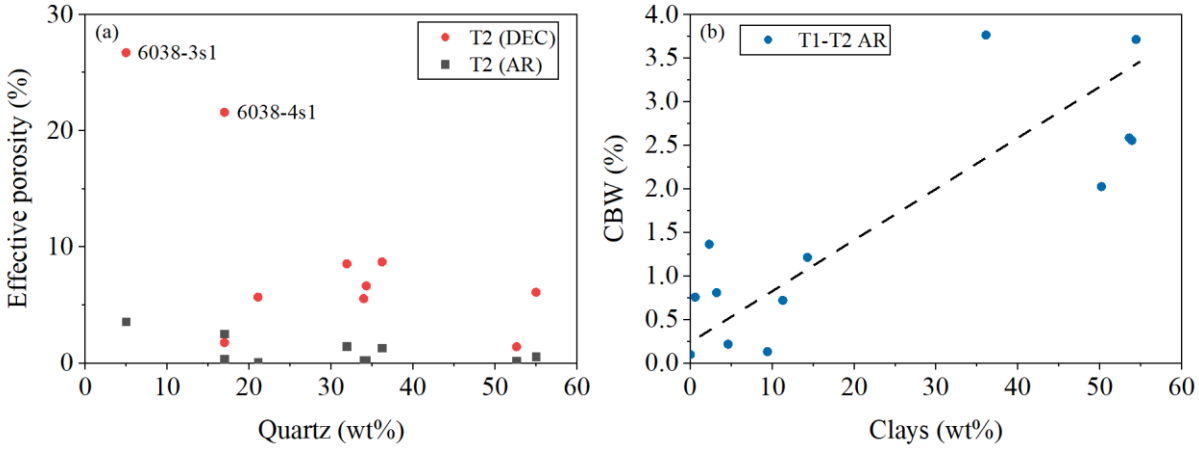

Fig. S9. Fluid-rock interaction: correlation between (a) quartz and (b) clay content and porosity of samples.

Fig. S10 shows that the sum of NMR porosity (hydrocarbon-filled voids) and gas porosity (empty pores) estimates total porosity close to post-extraction values (Fig., thus

minimizing solvent-induced alterations.

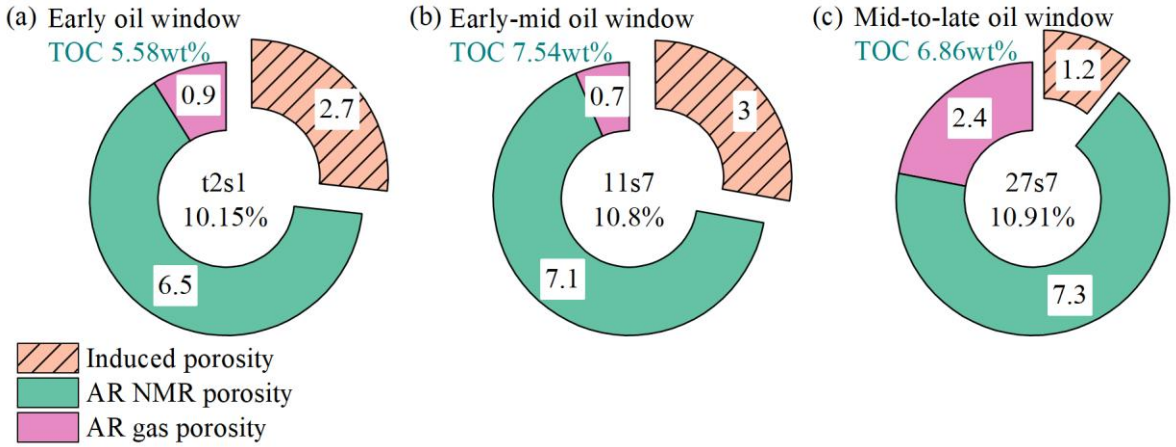

Fig. S10. Porosity reconstruction by combined analysis: (a) Sample t2s1, (b) sample 11s7, (c) sample 27s7. The total area corresponds to the producible NMR porosity (without residual fluids).

Appendix B: Tables

Four distinct lithotypes were identified in the investigated collection of Bazhenov Formation samples through an integrated analysis of thin sections, XRD, and XRF data; all results are in Tables S1 and S2.

Table S1. Elemental composition of the rock samples (XRF).

No.	LE (%)	Na_2O (%)	MgO (%)	Al_2O_3 (%)	SiO_2 (%)	K_2O (%)	CaO (%)	TiO_2 (%)	MnO (%)	$FeO + Fe_2O_3$ (%)	P_2O_5 (%)	S (%)
6s1	9.87	1.3	1.36	19.35	56.62	2.28	0.21	0.77	0.03	4.41	0.03	1.27
11s1	18.61	1.47	1.35	12.73	48.1	1.69	0.43	0.56	0.09	12.34	0.1	10.3
11s3	19.22	1.21	1.31	12.18	45.77	1.65	0.21	0.5	0.05	13.66	0.12	11.43
11s7	22.07	1.09	1.4	10.96	46.12	1.85	0.48	0.54	0.11	11.96	0.17	10.16
25s5	22.03	0.28	1.8	3.69	43.37	0.66	25.42	0.2	0.07	2.39	0.3	3.17
25s6	19.86	0.25	0.89	3.51	44.43	0.67	25.15	0.2	0.05	2.13	0.29	2.71
27s7	16.55	0.35	1.58	3.58	59.12	0.53	3.68	0.21	0.04	10.87	0.51	12.14
27s9	12.84	0.56	0.57	6.63	70.52	1.33	0.22	0.4	0.02	3.6	0.08	4.4
42s3	6.1	0.85	1.66	11.25	70.23	2.58	2.04	0.7	0.13	3.59	0.07	2.14
t2s1	14.4	1.96	2.99	11.97	48.97	2.19	7.28	0.84	0.08	4.59	0.27	4.44
t7s1	7.55	0.3	0.18	2.09	85.66	0.27	0.24	0.1	0.01	1.51	0.08	3.07
6038-3s1	36.97	0.15	0.9	1.6	9.13	0.23	45.28	0.09	0.03	2.04	0.29	2.7
6038-4s1	22.75	0.77	0.67	6.03	32.52	1.02	28.15	0.45	0.02	3.14	0.18	3.66

The XRD data (shown in Table S2) reveal a carbonate rock lacking primary sedimentary structures, likely due to extensive diagenetic

overprinting, including recrystallization and pervasive dolomitization.

Table S2. Mineral composition of the rock samples (XRD).

No.	Albite	Calcite	Chlorite	Dolomite	Illite	Kaolinite	Microcline	Montmorillonite	Pyrite	Quartz	Siderite	Smectite
6s1	4.2	0	7.5	0	19.9	25.7	7.1	0	0.6	34	0.2	0.8
11s1	7.3	0	5.1	0	30.4	13.3	0.8	0	5	36.2	0.5	1.4
11s3	4.6	0	3.7	0	29.3	10.7	7.4	8.2	2.5	31.9	0	1.7
11s7	12.5	0	6.1	0	28.6	15.9	1.9	3.8	10	21.1	0.1	0
25s5	1.2	51.8	0	15.6	7.3	0	1.8	4	1.3	17	0	0
25s6	5	34.2	0	2.1	3.2	0	1.2	0	1.7	52.6	0	0
27s7	2.1	0	1.5	12.1	0.9	2.2	2	0	5	74.2	0	0
27s9	5	0	0	0	1.7	0.6	9.9	0	1.8	81	0	0
42s3	6.2	2	1.8	0	21.8	3	0	7.9	0.7	55	0	1.6
t2s1	20.7	8.1	0.8	13.6	10.9	2.6	7.4	0	1.6	34.3	0	0
t7s1	0.9	0	0	0	0	0	5.9	0.6	0.6	92	0	0
6038-3s1	1.6	89	0	2.3	0	0	0.7	0	1.4	5	0	0
6038-4s1	9.5	57.5	0	1.9	8.9	0	3.4	0.5	1.3	17	0	0

To evaluate the OM characteristics of the Bazhenov Formation across three well locations, Rock-Eval pyrolysis was conducted on the core samples, results are shown in Table S3.

Table S3. Pyrolytic parameters of OM by Rock-Eval pyrolysis.

No.	S0	S1	S2	S3	TOC	Tmax	HI	OI	PI	CC	CaCO3	AI	OSI	GOC
	mg HC/g rocks	mg HC/g rocks	mg HC/g rocks	mg CO_2/g rocks	wt%	°C	mg HC/g TOC	mg CO_2/g TOC		wt%	wt%	%	Oil Saturation Index	wt %
6s1	0.59	1.67	5.83	0.29	2.07	446	282	14	0.28	0.11	0.89	1.71	109	0.77
11s1	1.41	5.79	16.46	0.38	6.42	443	256	6	0.3	0.18	1.52	5.3	112	2.18
11s3	1.64	5.13	12.09	0.23	6.02	446	201	4	0.36	0.15	1.25	4.97	112	1.78
11s7	2.4	4.23	13.79	0.62	7.54	445	183	8	0.32	0.29	2.42	6.22	88	1.99
25s5	2.48	2.64	12.14	0.44	6.4	451	190	7	0.3	5.08	42.37	5.28	80	1.72
25s6	2.47	4.31	12.08	0.53	7.08	447	171	7	0.36	4.36	36.32	5.84	96	1.87
27s7	2.89	11.42	13.26	0.78	6.86	444	193	11	0.52	0.93	7.72	5.66	209	2.68
27s9	3.42	6.29	11.84	0.27	7.03	438	168	4	0.45	0.09	0.73	5.8	138	2.16
42s3	0.17	3.67	7.86	0.18	1.69	435	233	20	0.29	0.34	2.84	1.05	94	0.4
t2s1	1.96	3.32	36.77	0.29	5.87	430	627	5	0.13	2.1	17.49	4.84	90	3.78
t7s1	6.55	21.52	21.26	0.72	6.57	435	324	11	0.57	0.16	1.34	5.42	427	4.81
6038-3s1	7.33	10.43	3.94	0.55	4.26	454	92	13	0.82	9.83	81.95	3.52	417	2.54
6038-4s1	6.22	15.37	12.89	0.49	8.12	459	159	6	0.63	4.6	38.33	6.7	266	3.51

The initial porosity values of the rock samples spanned a broad range from 0.6% to 24%, with an average porosity of approximately 3.97 % (median = 1.72%, n = 11) as shown in Table S4.

Table S4. Porosity and permeability of core plugs by gas.

No.	AR		AE-2		AE-3	
	Porosity (%)	Permeability (mD)	Porosity (%)	Permeability (mD)	Porosity (%)	Permeability (mD)
6s1	1.7	0.06	9.1	0.11	12.5	0.73
11s1	2.1	0.05	5.6	0.05	/	/
11s3	1.4	0.04	9	0.4	/	/
11s7	0.7	0.01	2.3	0.04	/	/
25s5	2.1	0	9.6	0.07	10.9	0.06
25s6	1.2	0.01	8.5	0.13	9.2	0.71
27s7	2.4	0.01	13.7	0.01	13.2	0.02
42s3	1.3	0.3	9.4	0.04	10.5	0.04
6038-3s1	24.6	11.92	32.1	19.12	32.3	24.82
t2s1	0.9	0.35	8.1	4.5	/	/
t7s1	5.3	0.02	10.2	0.03	/	/

Table S5 shows that for relatively permeable samples, μCT porosity (D = Ø4 mm) correlates well with gas porosity (D=Ø30 mm).

Table S5. Segmented porosity by μCT.

No.	Porosity (%)				Change in porosity (abs%)		
	AR	AE-1	AE-2	AE-3	AE-1 - AR	AE-2 - AE-1	AE-3 - AE-1
6s1	15.34	16.1	16.37	/	0.76	0.27	/
11s3	2.66	3.38	3.56	/	0.72	0.18	/
11s7	7.95	13.33	17.83	18.02	5.38	4.5	0.19
25s5	9.77	16.5	17.42	20.86	6.72	0.92	3.44
25s6	14.74	25.4	26.82	27.88	10.66	1.42	1.06

No.	Porosity (%)				Change in porosity (abs%)		
	AR	AE-1	AE-2	AE-3	AE-1 - AR	AE-2 - AE-1	AE-3 - AE-1
27s7	11.32	16.09	16.63	19.59	4.77	0.55	2.96
42s3	16.65	18.22	22.04	24.18	1.57	3.81	2.14
6038-3s1	27.79	29.12	30	33.23	1.33	0.89	3.23
t2s1	2.12	3.54	7.85	10.64	1.42	4.31	2.78

NMR analysis showed that total fluid saturation in AR samples reached up to 2.2 ml, corresponding to a maximum porosity of 11.5%, with an average porosity of 7.7 ± 2.6% (n = 13) as shown in Table S6.

Table S6. Saturation and porosity by NMR (T2 analysis).

No.	AR						AE-1	AE-2	AE-3	DEC							
	Fluid volume (ml)	Total Porosity (%)	CBW (%)	BVI (%)	FFI (%)	Effective porosity (%)	Fluid volume (ml)	Fluid volume (ml)	Fluid volume (ml)	Fluid volume (ml)	Total Porosity （%）	CBW (%)	BVI (%)	FFI (%)	Open porosity (%)	Grav porosity (%)	Effective porosity (%)
11s1	2.21	11.49	10.19	0.91	0.39	1.3	0.61	0.38	0.41	3.04	15.86	7.16	4.28	4.42	12.79	12.7	8.7
11s3	1.74	11.5	10.08	0.98	0.44	1.42	0.36	0.25	0.37	2.39	15.83	7.29	3.85	4.69	12.36	13.1	8.55
25s5	1.09	5.22	4.88	0.23	0.11	0.34	0.15	0.33	0.24	1.73	8.25	6.49	1.54	0.22	6.6	6.6	1.75
25s6	1.01	5.32	5.15	0.1	0.06	0.16	0.3	0.18	0.17	1.68	8.8	7.39	0.84	0.57	7.52	6.6	1.41
27s7	1.59	7.33	4.41	1.78	1.15	2.92	0.29	0.25	0.2	2.65	12.2	5.26	3.93	3.01	10.91	10.8	6.94
27s9	1.52	9.45	7.35	1.47	0.64	2.11	0.2	0.19	0.26	2.26	14.06	7.97	3.78	2.31	11.74	11.3	6.08
42s3	2.11	10.35	9.79	0.42	0.14	0.56	0.91	0.45	0.57	4.2	20.59	14.5	0.84	5.25	16.57	14.5	6.09
6038-3s1	1.01	4.88	1.33	1.88	1.67	3.56	0.04	0.05	0.15	5.82	28.18	1.47	1.26	25.44	27.11	30.1	26.71

No.	AR						AE-1	AE-2	AE-3	DEC							
	Fluid volume (ml)	Total Porosity (%)	CBW (%)	BVI (%)	FFI (%)	Effective porosity (%)	Fluid volume (ml)	Fluid volume (ml)	Fluid volume (ml)	Fluid volume (ml)	Total Porosity （%）	CBW (%)	BVI (%)	FFI (%)	Open porosity (%)	Grav porosity (%)	Effective porosity (%)
6038-4s1	1	4.6	2.09	1.74	0.77	2.51	0.13	0.14	0.13	5.12	23.62	2.03	4	17.59	22.77	24.9	21.59
t2s1	1.34	6.54	6.3	0.21	0.04	0.25	1.21	0.42	0.49	2.78	13.58	6.93	3.5	3.15	10.15	10.6	6.65
t7s1	1.98	9.89	4.14	4	1.75	5.75	0	0.26	0.14	3.02	15.11	1.96	0.98	12.17	14.14	14.9	13.15
11s7	1.45	7.1	7.01	0.05	0.03	0.09	0.75	0.47	0.37	2.73	13.35	7.66	2.7	2.99	10.8	11.3	5.69
6s1	1.35	6	5.77	0.23	0.01	0.23	0.44	0.31	0.43	2.5	11.09	5.54	3.09	2.46	8.39	8.3	5.54

Gravimetric porosity after Decane saturation showed the best consistency with open porosity (R2=0.9946), confirming the accuracy and precision of the NMR results as shown in Table S7.

Table S7. Gravimetric porosity of Decane-saturated rock samples.

No.	Mass of dry sample before saturation (g)	Mass of saturated sample in air (g)	Mass of saturated sample in decane (g)	Open porosity (%)
25s5	50.7939	51.8003	36.4887	6.6
11s1	47.2943	49.1528	34.4917	12.7
t7s1	43.3473	45.4944	31.0392	14.9
27s7	50.4668	52.1829	36.3483	10.8
42s3	51.0172	53.3268	37.3858	14.5

No.	Mass of dry sample before saturation (g)	Mass of saturated sample in air (g)	Mass of saturated sample in decane (g)	Open porosity (%)
6038-3s1	38.0962	42.5581	27.7575	30.1
6038-4s1	41.2484	45.0114	29.8953	24.9
t2s1	47.0387	48.6801	33.1482	10.6
11s7	48.7838	50.5208	35.1331	11.3
27s9	37.2192	38.5652	26.6686	11.3
11s3	36.8811	38.3756	26.983	13.1
25s6	45.0053	45.9048	32.2181	6.6
6s1	51.2102	52.4751	37.2881	8.3

To separate the hydrogen populations and identify the fluid types, two-dimensional NMR T_1–T_2 maps were constructed for samples immediately after unpacking the tubes; results are in Table S8.

Table S8. Fluid grouping by NMR (T_1-T_2 analysis)

No.	AR			AE-1			AE-2			AE-3			DEC		
	Viscous and adsorbed HC (%)	Clay-bound water. %	Mobile fluids (%)	Viscous and adsorbed HC (%)	Clay-bound water. %	Mobile fluid (%)	Viscous and adsorbed HC (%)	Clay-bound water. %	Mobile fluids (%)	Viscous and adsorbed HC (%)	Clay-bound water. %	Mobile fluids (%)	Viscous and adsorbed HC (%)	Clay-bound water. %	Mobile fluids (%)
11s1	75.9	17.6	6.5	50.7	47.8	1.5	26.4	70.2	3.4	23.6	73	3.4	55.8	12.6	31.6
11s3	71.4	22.5	6.2	27.5	71.9	0.6	49.1	47.4	3.5	16.2	79.1	4.7	50.3	12.6	37.1
25s5	82.7	13.8	3.5	66.5	25.8	7.6	51.4	40.2	8.4	56.6	34.6	8.8	76.4	17.1	6.5

No.	AR			AE-1			AE-2			AE-3			DEC		
	Viscous and adsorbed HC (%)	Clay-bound water %	Mobile fluids (%)	Viscous and adsorbed HC (%)	Clay-bound water %	Mobile fluid (%)	Viscous and adsorbed HC (%)	Clay-bound water %	Mobile fluids (%)	Viscous and adsorbed HC (%)	Clay-bound water %	Mobile fluids (%)	Viscous and adsorbed HC (%)	Clay-bound water %	Mobile fluids (%)
25s6	82.5	15.2	2.3	65.7	33	1.3	55.2	40.9	3.9	52.1	37.6	10.3	68.7	22.4	8.9
27s7	73.8	3	23.2	76.2	18.4	5.5	69.5	24.9	5.6	58.2	32.2	9.6	61.4	13.5	25.1
27s9	73.9	14.4	11.6	55.6	41.7	2.6	52.4	44.8	2.8	51.8	41.2	7	66.4	14.1	19.5
42s3	60.3	36.4	3.3	11.7	87.1	1.2	26.4	70.1	3.6	17.3	78.9	3.8	22.9	49.6	27.5
6038-3s1	55.2	2.1	42.7	71.3	16.3	12.4	63	20.4	16.7	46	32.1	21.9	11.9	2	86.1
6038-4s1	70.7	2.9	26.4	63	29.9	7.1	46.1	43.8	10.2	32.1	50	17.9	19	1.5	79.5
t2s1	79.6	18.5	1.9	81.1	14.9	4	39.8	57.4	2.8	52.3	43.9	3.8	63.7	9	27.3
t7s1	64.6	7.7	27.7	83.5	3.2	13.3	78.4	12.1	9.5	67.6	15	17.3	19	1.5	79.5
11s7	46.5	52.4	1.2	50.5	48.7	0.8	20.8	77	2.2	23.1	71.7	5.2	53.1	22.9	23.9
6s1	56.6	42.6	0.8	28.9	70	1.1	29.6	69	1.4	28.8	66.8	4.3	56.8	15.9	27.3

Table S9 illustrates that most hydrocarbons in the rock were removed during AE-1 step using hexane for mature samples. The chloroform proved its efficiency in subsequent core cleaning, especially for low mature clay-siliceous and siliceous mudstone samples with high TOC and clay content.

Table S9. Mass of core samples during the multistage extraction

No.	Before extraction	AE-1		AE-2		AE-3	
	Mass of sample (g)	Mass of sample (g)	Relative mass of extract (mg/g)	Mass of sample (g)	Relative mass of extract (mg/g)	Mass of sample (g)	Relative mass of extract (mg/g)
11s3	37.2641	37.03557	6.1326	36.7008	2.1629	36.59778	2.806986
11s7	49.2933	49.24503	0.9792	49.0848	4.9865	48.7968	5.86744
6038-4s1	42.0726	41.42309	15.4377	41.2863	1.6685	41.10972	4.276856
42s3	51.4017	51.37852	0.4509	50.9115	0.0759	50.88546	0.511527
25s5	51.3932	51.12994	5.1225	50.9033	2.9751	50.78307	2.361921
t7s1	45.1295	44.6104	11.5024	43.4463	4.5335	43.4027	0.468501
27s7	51.3071	50.71694	13.2075	50.3462	2.7184	50.32261	1.267272
27s9	37.8158	37.31635	8.2744	37.0484	0.793	37.00145	1.635348
6s1	53.3449	52.9035	18.5908	51.1161	1.2369	51.03251	1.150797
6038-3s1	38.8404	38.11832	2.0848	38.0733	4.6035	38.02949	1.060589
25s6	45.3338	45.23929	2.6582	44.9843	4.1965	44.93659	3.491413
11s1	47.6406	47.51396	5.8482	47.3195	15.9146	47.15429	3.503558
t2s1	47.9011	47.62097	6.1326	46.85864	2.1629	47.73328	2.806986